JOURNAL OF MATERIALS SCIENCE 28 (1993) 155–160

Evaluation of the fracture toughness of Nb–40Al–8Cr–1W–1Y–0.05B intermetallic material by indentation techniques

S. R. CHOI, J. A. SALEM
National Aeronautics and Space Administration, Lewis Research Center, Cleveland, OH 44135, USA

M. G. HEBSUR
Sverdrup Technology, Inc., Lewis Research Center Group, Brook Park, OH 44142, USA

The fracture toughness of an Nb–40Al–8Cr–1W–1Y–0.05B intermetallic material was evaluated by indentation techniques at room temperature. Two widely used indentation methods, crack size measurement and indent strength, yielded excellent agreement with a conventional fracture toughness technique using straight-through precracked specimens, despite the occasional formation of poorly configured cracks. However, the modified indentation technique, using dummy indent flaws, resulted in a low fracture toughness compared to that evaluated by the other methods. The material did not exhibit rising *R*-curve behaviour, as evaluated from the indentation strength data. These results indicate that indentation fracture principles are applicable to this brittle intermetallic material without modification of the residual contact stress term originally calibrated for ceramic materials.

1. Introduction

The use of identation flaws is well established for studying the mechanical properties of glasses and ceramics. The attraction of indentation techniques is their simplicity as a means of introducing a small, predetermined flaw configuration into test specimens. In particular, indentation techniques have been utilized to evaluate the fracture toughness of ceramic materials for more than a decade, although indentation analysis is not theory-oriented in a rigorous sense because of the complexities associated with elastic/plastic deformation of the indentation.

The indentation toughness techniques are typically divided into two categories: crack size measurement [1] and indentation strength [2] methods. The former technique is based on the lengths of the cracks emanating from the corners of Vickers microhardness indents. This technique is popular due to the ease of application to very small specimens. The latter technique depends on the strength measurements of indented specimens with no need to measure crack length, but requires several specimens with sufficient volume (approximately 300 mm^3). In either case, the success of these indentation techniques is dependent on the brittleness of the test material and the formation of well-configured indentation cracks.

In the present work, the indentation techniques were extended to evaluate the fracture toughness of a brittle, $NbAl_3$ base intermetallic material (Nb–40Al–8Cr–1W–1Y–0.05B). Fracture toughness was evaluated at room temperature using the widely applied methods of crack size measurement [1] and indentation strength [2]. The fracture toughness values thus evaluated were compared to those obtained by a more conventional fracture toughness specimen (single-edge-precracked-beam method). To our knowledge, this is the first comparison of the indentation approach to conventional fracture toughness measurements of an intermetallic material. The motive to use indentation techniques stems from the fact that the material is brittle in nature, and that the availability of the material was insufficient for fabrication of conventional fracture toughness specimens (chevron notch, compact tension, or double cantilever beam) due to its novel fabrication process.

2. Indentation fracture

The basic underlying theory of indentation response in brittle materials is briefly reviewed here. For indentation cracks produced in brittle materials by a Vickers microhardness indentor, the mode I stress intensity factor, K_R, representing a half-penny crack configuration, results from the residual stress field of the elastic/plastic mismatches of indentation [3]. The residual driving force, K_R, is primarily responsible for expanding the crack system into the final equilibrium penny-shaped configuration. For a well-developed crack, where the crack size is larger than the deformation size, the crack system may be considered as centre-loaded by a residual stress field at the deformation zone of indentation. Consequently, the corresponding residual driving force is [4]

$$K_R = \sum_r P/c^{3/2} \quad (1)$$

0022–2461

where Σ_r is a dimensionless constant, P is the indentation load, and c is the indentation crack size measured from the centre of the indent to the crack tip. The constant Σ_r, associated with the residual stresses, was evaluated via plasticity analysis of an expanding spherical cavity by Hill [5], and shown to dependent on hardness, H, Young's modulus, E, and indentor geometry

$$\sum_r = \phi(E/H)^{1/2} \quad (2)$$

where ϕ is an indentor geometry-dependent constant which was determined for a Vickers indentor to be $\phi = 0.016 \pm 0.004$ for various ceramics [1]. Hence, in the post-indentation equilibrium condition at $c = c_0$ and $K_R = K_c$ (toughness), Equation 1 reduces to

$$K_c = 0.016(E/H)^{1/2} P/c_0^{3/2} \quad (3)$$

where c_0 is the post-indentation crack size without fatigue effects. This is an equation for evaluating fracture toughness based on the measurements of post-indentation crack size, c_0, as a function of indentation load, P, with known E and H.

If an indentation crack is subjected to an applied tensile stress, σ_a, the net stress intensity factors consists of two components

$$K = K_R + K_a = \sum_r P/c^{3/2} + \Omega\sigma_a c^{1/2} \quad (4)$$

where K_a is the mode I stress intensity factor resulting from the tensile stress, expressed as $K_a = \Omega\sigma_a c^{1/2}$ with Ω being the crack geometry factor. The functional dependency of K on c indicates that precursor stable crack growth with conditions of $K \geqslant K_c$ and $dK/dc < 0$ occurs during loading until the instability point where $K = K_c$ and $dK/dc = 0$. Using this instability condition, one can obtain [3]

$$\sigma_f = 3K_c/(4\Omega c_f^{1/2}) \quad (5a)$$

$$c_f = (4\sum_r P/K_c)^{2/3} \quad (5b)$$

where σ_f and c_f are, respectively, the fracture strength and the critical crack size at failure. Therefore, the precursor stable crack growth occurs from the as-indented crack size; c_0, to the final crack size, c_f, due to the residual stress field. Also, from Equations 5a, b and 2, one can obtain the fulfilling toughness equation

$$K_c = \mu(E/H)^{1/8}(\sigma_f P^{1/3})^{3/4} \quad (6)$$

where $\mu = (256\phi\Omega/27)^{1/4}$ is another geometrical constant, which was calibrated to be $\mu = 0.59 \pm 0.12$ for various ceramic materials [6]. Therefore, with known E and H, the fracture toughness can be determined from Equation 6 once indentation strength, σ_f, is known as a function of indentation load, P. As a consequence, this technique is called the indentation strength method.

It is also noted that toughness can also be evaluated from the indentation strength and critical crack size data, as can be seen in Equation 5a. The critical crack size, c_f, can be estimated by a dummy indentation technique [6] or by direct measurements from the fracture surface. In the dummy indentation technique, four or five indents are placed on the prospective tensile surface within the inner span of a four-point fixture. During strength testing the cracks are subjected to precursor stable crack growth, eventually resulting in failure from only one indent, leaving the other intact dummy indent cracks available for the measurement of c_f. Based on this dummy indent technique together with Equation 5a, Cook and Lawn [6] obtained an empirical equation for K_c for various ceramic materials

$$K_c = A\sigma_f c^{1/2} + B \quad (7)$$

where $A = 2.02$ and $B = -0.68$ MPa m$^{1/2}$. This technique is termed the modified indentation technique [6].

3. Experimental procedure

3.1. Material and specimens

The material used in this study was an $NbAl_3$-base intermetallic material with the composition Nb–40Al–8Cr–1W–1Y–0.05B (wt %) produced by rapid solidification processing (RSP) and hot isostatic pressing (HIP) at NASA Lewis Research Center. The detailed material processing was reported elsewhere [7]. The physical properties of this material are summarized in Table I. All the specimens were in the form of MOR bars with nominal dimensions of 3 mm by 4 mm by 20 mm. The specimens were polished with 5 μm alumina to obtain mirror surfaces appropriate for indentation.

3.2. Indentation tests

Each specimen was indented for 15 s in room-temperature air with a Vickers microhardness indentor in the centre of the polished surface with the indentation diagonals parallel and perpendicular to the direction of prospective tensile stress. Four indents were placed on the tensile surface within the inner span of a four-point bend fixture, with 1.5 mm spacing between each indent to minimize possible crack interactions. After indentation, the crack sizes were measured using an optical microscope attached to the hardness tester. Three to four indentation loads of $P = 49$–206 N were used. Three test specimens were used at each indentation load.

After measuring post-indentation crack sizes, c_0, the indented specimen (containing four indents) was fractured using a four-point bend fixture with 18/10 mm spans in a testing machine using a cross-head speed of 0.2 mm min^{-1}. The crack sizes of the surviving dummy indents were measured optically. In

TABLE I Physical properties of intermetallic test material. Parentheses indicate ± 1.0 S.D.

Young's modulus, E[a] (GPa)	Hardness, H[b] (GPa)	Density (g m^{-3})
213.7 (6.0)	6.75 (0.09)	4.5

[a] Evaluated by strain gauging.
[b] Evaluated by Vickers indentor; three indent loads of 98, 147 and 206 N with three indents per load.

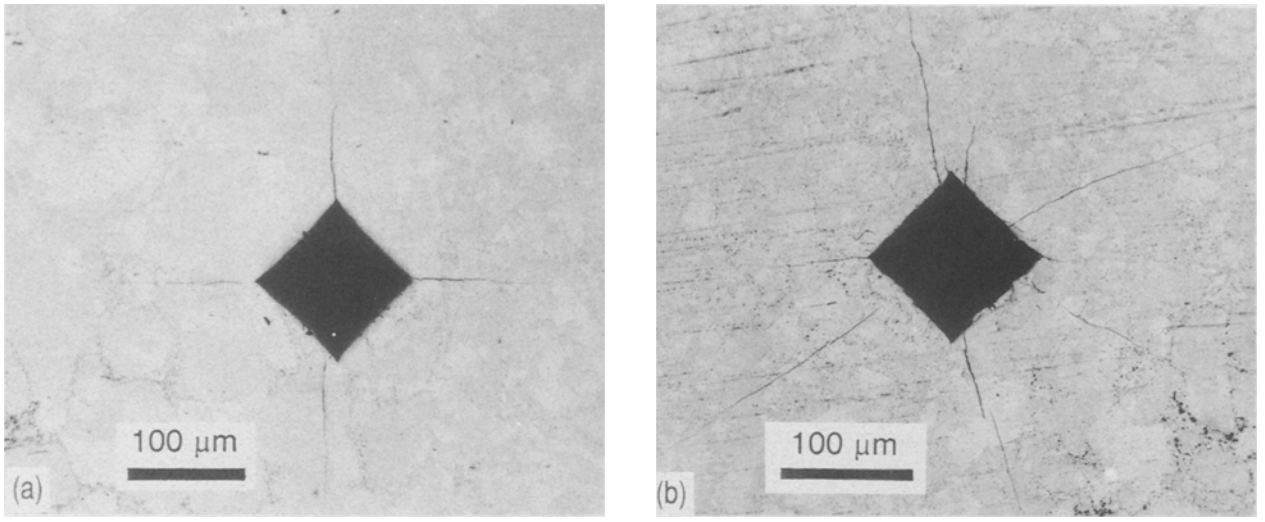

Figure 1. Typical indent crack configurations produced on specimen surfaces: (a) acceptable and (b) unacceptable crack patterns.

addition, the critical crack sizes were also determined from the fracture surfaces of the specimens.

3.3. SEPB tests

In the single-edge precracked-beam (SEPB) method [8], an indent was placed in the centre of the polished specimen surface using an indentation load of 98 N in the manner described earlier. The indented specimen was then placed in a precracking fixture and loaded via the testing machine to produce gradually a controlled increasing tensile stress at the indent site until the indentation crack popped-in to form a straight-through precrack. The precrack size for a given material depends on both indentation load and fixture span. A span of 4 mm was used. Detailed analysis of precracking parameters for SEPB ceramic specimens has been made recently by Choi *et al.* [9]. After precracking, the specimens were broken at a crosshead speed of 0.2 mm min^{-1} with the fixture used in the indentation strength testing. An average crack length was obtained at three points on the fracture surface: at the centre of the crack front, and at the quarter-thickness points, as described in the standard plane strain fracture toughness method for metals [10]. Five specimens of nine were determined to be acceptable based on the requirements specified in the standard. Fracture toughness, K_c, was evaluated using the formula [11]

$$K_c = \frac{3FL}{tW^2}(\pi a)^{1/2} F_{IM}(\alpha) F_{IP} \quad (8)$$

with

$$F_{IM}(\alpha) = 1.122 - 1.121\alpha + 3.740\alpha^2 + 3.873\alpha^3 - 19.05\alpha^4 + 22.55\alpha^5$$

where F is the fracture load, $L = (L_o - L_i)/2$ with L_o and L_i being the outer and inner span of the test fixture, respectively. The precrack size, specimen thickness, specimen width, and normalized crack length are a, t, W, and $\alpha = a/W$. F_{IP} is a correction factor depending on a/W and L_i/W, and approaches unity when $L_i/W \geq 2.5$ regardless of a/W.

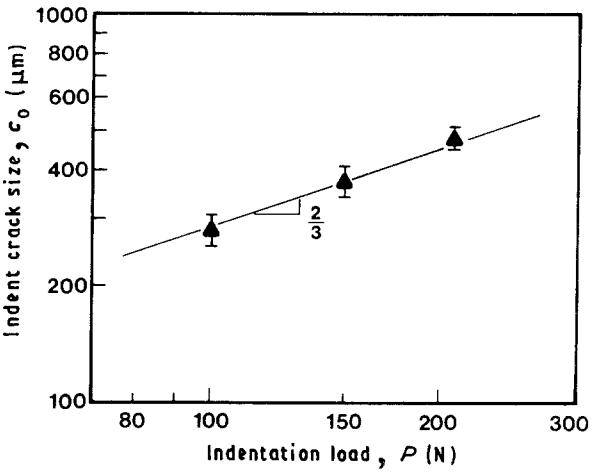

Figure 2. Post-indentation crack size ($\log c_0$) as a function of indentation load ($\log P$). (——) Best-fit line with a slope of 2/3. The error bar indicates ± 1.0 S.D.

4. Results and discussion

Typical indentation cracks produced on the test specimens are presented in Fig. 1, where a well-defined crack pattern is compared with an ill-defined crack pattern. The indentation impression in this material was always well developed, presumably due to its low hardness (H = 6.75 GPa). However, the radial cracks emanating from the indentation corners were not always well-configured, sometimes varying in number from three to eight with appreciable variances in their size. This irregular indentation cracking was similar to that occurring in SiC materials or aluminas with large grains. About 30% of the cracks were of ill-defined configuration, independent of indentation loads from 48–206 N. All the crack size measurements that were necessary to calculate fracture toughness were performed only for well-configured cracks.

Fig. 2 shows results of the crack-size measurements as a function of indentation load. The solid line represents a line force-fitted to the data with a slope of 2/3 in $\log c_0$ versus $\log P$, based on Equation 3. The functional fit analysis resulted in $P/c_0^{3/2} = 0.02040 \pm 0.00052$ N $\mu m^{-3/2}$, with a correlation coefficient of 0.9510. Using this value of $P/c_0^{3/2}$ together with the

TABLE II Summary of fracture toughness evaluated by different indentation techniques. Parentheses indicate ± 1.0 S.D.

Load, P (N)	Method					
	Crack size		Indent strength		Modified indentation	
	C_0 (μm)	K_c (MPa m$^{1/2}$)	σ_f (MPa)	K_c (MPa m$^{1/2}$)	K_c[a] (MPa m$^{1/2}$)	K_2[b] (MPa m$^{1/2}$)
68.6	–	–	68(10)	1.95(0.23)	–	–
98.1	276(27)	1.93(0.28)	61(10)	1.98(0.07)	1.44	1.52
147.0	377(30)	1.81(0.21)	58(2)	2.09(0.25)	1.75	1.70
206.0	478(36)	1.77(0.20)	46(8)	1.92(0.22)	1.38	1.46
All loads		1.84		1.99	1.52	1.56
		(0.08)		(0.07)	(0.07)	(0.12)

[a] From fracture surface measurements.
[b] From dummy indent crack measurements.

values $E = 214$ GPa and $H = 6.75$ GPa (Table I), fracture toughness was calculated using Equation 3 to be $K_c = 1.84 \pm 0.08$ MPa m$^{1/2}$. The individual crack-size data as a function of indentation load are also tabulated in Table II. Although the variation in crack size for each indentation load was greater than that typical of glasses and silicon nitride ceramics, the overall fracture toughness was consistent regardless of indentation loads applied, implying that indentation behaviour of the intermetallic material follows indentation theory very well.

Results of the indentation strengths as a function of indentation load are depicted in Fig. 3, where a decrease in indentation strength with increasing indentation load is evident. The solid line in the figure represents a forced-fit line with a slope of $-1/3$ in a plot of log σ_f versus log P, based on Equation 6. The forced-fit analysis yielded a value of $\sigma_f P^{1/3} = 283.86 \pm 7.14$ MPa N$^{1/3}$ with a correlation coefficient of 0.9528, indicating that the response of indentation strength to indentation load agrees quite well with indentation fracture theory. The use of the evaluated $\sigma_f P^{1/3}$ in Equation 6 with the estimated E and H values resulted in fracture toughness of $K_c = 1.99 \pm 0.07$ MPa m$^{1/2}$, which is very close to K_c ($= 1.84$ MPa m$^{1/2}$) evaluated by the crack-size measurement method. The individual toughness value for each identation load is also listed in Table II. A typical fracture surface showing a well-defined half-penny shaped crack is shown in Fig. 4. It was confirmed that all the failure-causing flaws were half-penny shaped cracks, validating the use of the fracture toughness equations (Equations 3 and 6) that are based on the assumption of a half-penny crack configuration.

The fracture toughness obtained by the modified indentation technique [6] is also presented in Table II, where K_cs based on the critical crack size, c_f, measurements from both the fracture surfaces and the dummy indent cracks are included. In general, K_c using this method was about 20% lower than that obtained by either the crack-size measurement or indentation strength method ($K_c = 1.52 \pm 0.20$ and 1.56 ± 0.12 MPa m$^{1/2}$), respectively, by the fracture surface and dummy indent crack measurements). This discrepancy in K_c is large, presumably due to the increased uncertainty in c_f measurements complicated by ill-defined crack tip regions.

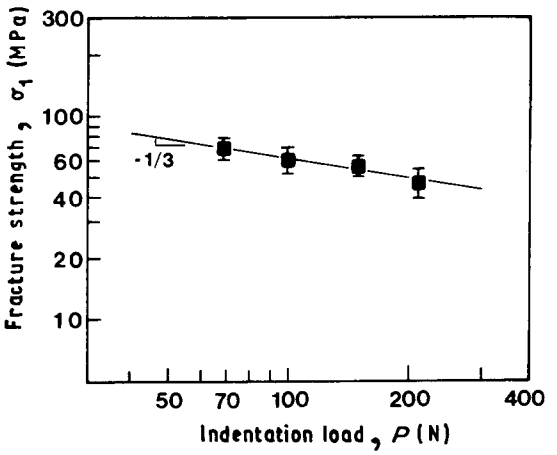

Figure 3. Post-indentation strength (log σ_f) as a function of indentation load (log P). (——) Best-fit line with a slope of $-1/3$. The error bar indicates ± 1.0 S.D.

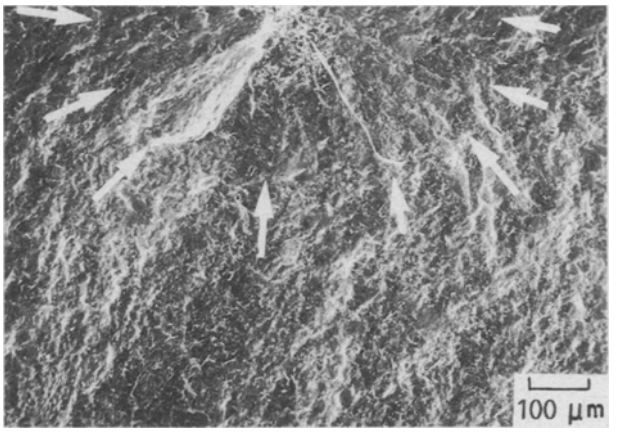

Figure 4. A typical fracture surface showing a well-developed half-penny crack configuration.

In the SEPB method, ill-configured indentation crack patterns on the specimen surfaces frequently resulted in unacceptable straight-through cracks which were invalid for evaluating fracture toughness. The K_c for the five specimens with acceptable pre-cracks was $K_c = 1.94 \pm 0.15$ MPa m$^{1/2}$. A typical

fracture surface of a SEPB specimen is shown in Fig. 5, where the precrack is clearly demarcated.

A summary of the fracture toughness values evaluated by crack-size measurement, indentation strength, modified indentation technique, and SEPB methods is presented in Fig. 6. It is apparent that good agreement exists between the crack size measurement, indentation strength and SEPB methods. On the other hand, the results obtained by the modified indentation technique were not consistent with other experimental results. Hence, the modified indentation technique would be seen as supplementing rather than replacing the other indent techniques, as noted previously [6]. Therefore, it can be concluded that the two widely used indentation methods, crack size measurement and indentation strength, can be used to evaluate fracture toughness of this intermetallic material within the range of indentation loads applied in this work. This means that indentation response of this material follows the indentation fracture principle without recalibration of the Σ_r constant. Between the two indentation methods, however, the strength method is preferred because of the elimination of the complicated crack size measurements which result in increased uncertainty.

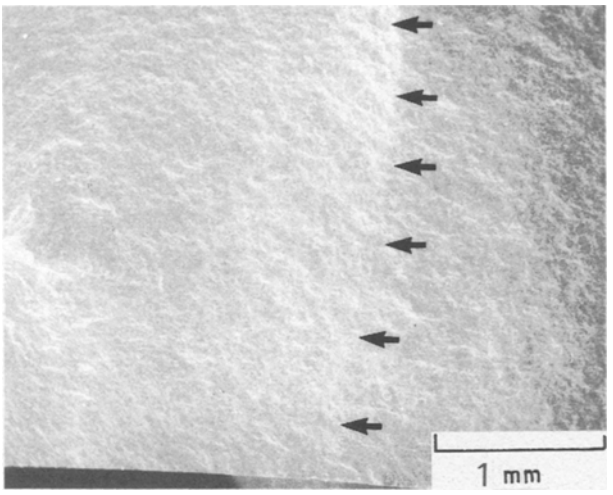

Figure 5. A typical surface of a straight-through precracked specimen (SEPB).

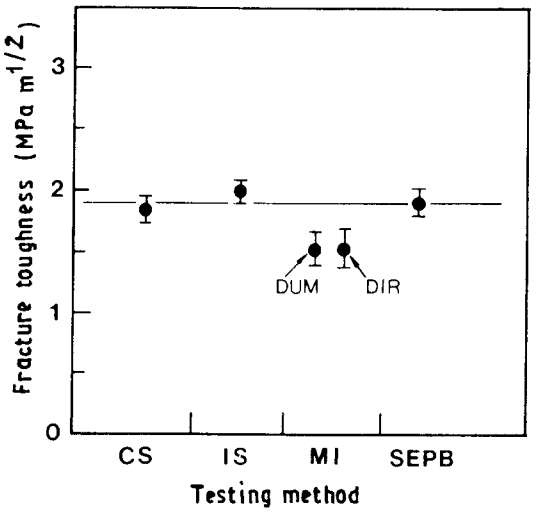

Figure 6. A summary of fracture toughness evaluated by four different methods: CS, crack size measurement; IS, identation strength; MI, modified indentation; (DUM, from dummy indent cracks; DIR, from fracture surfaces); SEPB. The horizontal line represents an average toughness (= 1.92 ± 0.08) obtained from CS, IS and SEPB methods.

The indentation fracture toughness techniques could be extended to other intermetallic materials, provided that the materials exhibit limited ductility and well-developed crack configurations. An attempt to apply indentation techniques to a more ductile intermetallic, NiAl with AlN precipitates, however, was not successful as no cracks were formed from the corners of indents. The material, instead, exhibited intergranular microcracking at triple points and pores around the indent. Thus, for materials that exhibit significant microcracking or local ductility, the indentation techniques are not applicable.

Because the $NbAl_3$ material follows indentation theory well, it may be feasible to estimate R-curve behaviour from the indentation strength data using the method by Krause [12]. The fracture resistance, K_r, is assumed to be related to the crack size, c, by a power-law relationship. The fracture resistance and the indentation strength relation are [12]

$$K_r = k c^m \tag{9a}$$

$$\sigma_f = A P^{2m-1/2m+3} \tag{9b}$$

with

$$A = \frac{k(3 + 2m)}{4\Omega}\left[\frac{4\sum_r}{k(1 - 2m)}\right]^{2m-1/2m+3} \tag{10}$$

where k and m are the material constants to be evaluated. Equation 9b reduces to Equation 5, for the case of no crack resistance toughening. Also, $K_r = K_c$ for $m = 0$. The toughening exponent, m, was evaluated for the best-fit slope of $\log \sigma_f$ versus $\log P$ data shown in Fig. 3. The constant k was determined from Equation 9a with the estimated m and the toughness value obtained from the indentation strength method for

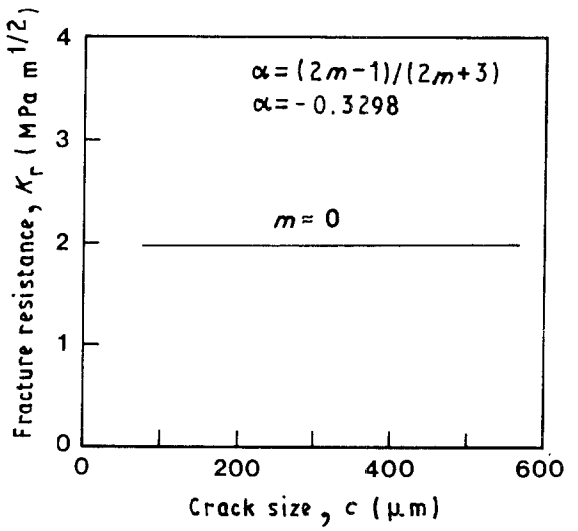

Figure 7. A predicted fracture resistance curve for the intermetallic material. Here α represents the best-fit slope in the plot of $\log \sigma_f$ versus $\log P$.

a given indentation crack size. The R-curve thus estimated is presented in Fig. 7. It can be seen from this figure that the material exhibits a flat R-curve and a negligible toughening exponent of $m \approx 0$, because the best-fit slope ($\alpha = -0.3298$) is very close to $-1/3$, which is the case of a flat R-curve. The flat R-curve was also evident from the crack trajectories that showed no significant crack deflection, bridging, and/or interlocking, as is the case for some brittle materials that exhibit a rising R-curve, such as ceramics.

5. Conclusions

Indentation techniques were applied to evaluate the fracture toughness of an $NbAl_3$ base intermetallic of composition Nb–40Al–8Cr–1W–1Y–0.05B. Although well-defined indent crack configurations were not always achievable, the two widely utilized methods (indent crack size measurement and indentation strength) yielded excellent agreement in fracture toughness with a more conventional fracture toughness method using precracked specimens (SEPB method). Fracture toughness was determined to be $K_c = 1.84$, 1.99, 1.94 MPa $m^{1/2}$, respectively, by the indent crack size measurement, indentation strength, and SEPB methods. The modified indent technique, however, yielded a lower value of $K_c = 1.54$ MPa $m^{1/2}$. The R-curve, evaluated from the indentation strength data, was not observed to rise in this material system. The above results indicate that the indentation fracture principle is applicable to this brittle intermetallic material for evaluating toughness, strength, and the R-curve without modification of the residual stress term.

Acknowledgement

The authors thank Mr R. Pawlik for experimental work during the course of this research.

References

1. G. R. ANSTIS, P. CHANTIKUL, B. R. LAWN and D. B. MARSHALL, *J. Amer. Ceram. Soc.* **64** (1981) 533.
2. P. CHANTIKUL, G. R. ANSTIS, B. R. LAWN and D. B. MARSHALL, *ibid.* **64** (1981) 539.
3. D. B. MARSHALL, B. R. LAWN and P. CHANTIKUL, *J. Mater. Sci.* **14** (1979) 2225.
4. B. R. LAWN, A. G. EVANS and D. B. MARSHALL, *J. Amer. Ceram. Soc.* **63** (1980) 574.
5. R. HILL, "The Mathematical Theory of Plasticity" (Oxford University Press, London, 1950) pp. 97–106.
6. R. F. COOK and B. R. LAWN, *J. Amer. Ceram. Soc.* **66** (1983) C200.
7. M. G. HEBSUR, I. E. LOCCI, S. V. RAJ and M. V. NATHAL, *J. Mater. Res.* (1992) 1696.
8. T. NOSE and T. FUJII, *J. Amer. Ceram. Soc.* **71** (1988) 328.
9. S. R. CHOI, A. CHULYA and J. A. SALEM, *Fract. Mech. Ceram.* **10** (1992) 73.
10. "Standard Test Method for Plane-Strain Fracture Toughness of Metallic Materials", ASTM Standard E399-90 (American Society for Testing and Materials, Philadelphia, PA, 1990).
11. Y. MURAKAMI, "Stress Intensity Factors Handbook", Vol. 1 (Pergamon Press, New York, 1987) pp. 16–17.
12. R. F. KRAUSE, *J. Amer. Ceram. Soc.* **71** (1988) 388.

Received 19 November 1991
and accepted 18 March 1992